THE JOURNAL OF PHYSICAL CHEMISTRY B

Article

pubs.acs.org/JPCB

Complete Solvation Response of Coumarin 153 in Ionic Liquids

Xin-Xing Zhang,[†,‡,∥] Min Liang,[§,∥] Nikolaus P. Ernsting,[‡] and Mark Maroncelli*[,§]

[†]Department of Physics, College of Physical Science, Nankai University, Tianjin, China

[‡]Department of Chemistry, Humboldt University, Berlin, Germany

[§]Department of Chemistry, The Pennsylvania State University, University Park, Pennsylvania, United States

Supporting Information

ABSTRACT: The dynamic Stokes shift of coumarin 153, measured with a combination of broad-band fluorescence upconversion (80 fs resolution) and time-correlated single photon counting (to 20 ns), is used to determine the complete solvation response of 21 imidazolium, pyrrolidinium, and assorted other ionic liquids. The response functions so obtained show a clearly bimodal character consisting of a subpicosecond component, which accounts for 10−40% of the response, and a much slower component relaxing over a broad range of times. The times associated with the fast component correlate with ion mass, confirming its origins in inertial solvent motions. Consistent with many previous studies, the slower component is correlated to solvent viscosity, indicating that its origins lie in diffusive, structural reorganization of the solvent. Comparisons of observed response functions to the predictions of a simple dielectric continuum model show that, as in dipolar solvents, solvation and dielectric relaxation involve closely related molecular dynamics. However, in contrast to dipolar solvents, dielectric continuum predictions systematically overestimate solvation times by factors of at least 2−4.

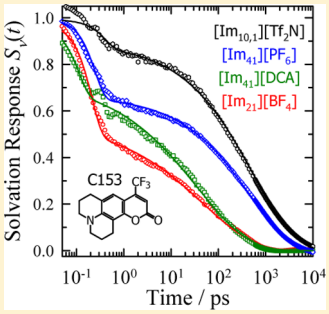

1. INTRODUCTION

Ionic liquids are a relatively new type of material of considerable interest both for their potential utility in numerous applications and as media wherein one might expect to discover new and distinctive solvent effects. For example, ionic liquids are finding use as solvents for organic and inorganic synthesis,[1,2] as media for analytical separations,[3,4] and in energy-related applications,[5] such as in biomass conversion,[6] fuel cells,[7] supercapacitors,[8,9] batteries,[7,10] and solar cells.[11,12] Partly in support of these applications, there has been a great deal of effort directed toward achieving a basic understanding of the physical properties and solvent characteristics of these liquids.[13−15] Of particular interest in the present work is the phenomenon known as "solvation dynamics", the way in which a medium responds to perturbations in the charge distribution of a solute. This solvation response is a fundamental characteristic of polar liquids. It is intimately related to frictional effects on solute motion and charge-transfer processes[16] and therefore relevant for a number of the applications mentioned above.[17]

Numerous studies of solvation dynamics in ionic liquids[18] using experimental,[17,19−26] computational,[27−32] and theoretical[33−35] approaches have been published over the past decade. As a result, the basic features of the solvation response in these interesting fluids are now reasonably well established. In contrast to simple dipolar liquids where solvation is typically over in a few picoseconds,[36] complete solvation in ionic liquids requires nanosecond or greater times. Nevertheless, in most cases a large fraction of the solvation response occurs faster (<10 ps) than can be captured by the picosecond techniques. In fact, simulations show that a substantial fraction of solvation occurs in the subpicosecond time domain. For this reason both ∼100 fs resolution and a ∼10 ns time window are needed to completely capture the dynamics of solvation in ionic liquids. To date, the fast solvation response has been probed using several techniques[37−40] and its subpicosecond time scale confirmed. A few groups have also combined fs/ps techniques in order to record the complete solvation response in several ionic liquids, but such data are relatively scarce.[41,42,38,43,44]

The present work seeks to provide a more comprehensive and improved experimental characterization of the solvation response in ionic liquids. For this purpose we employ the benchmark solute coumarin 153 (C153) and measure its dynamic Stokes shift using a combination of broadband fluorescence upconversion (FLUPS) and time-correlated single photon counting (TCSPC) spectroscopies. The former technique provides 80 fs resolution for times up to 650 ps and the latter extends this coverage out to times of 20 ns in order to ensure that the full solvation response has been captured. A total of 21 common, nonfunctionalized imidazolium, pyrrolidinium, and assorted other ionic liquids are included here. We also examine the accuracy of a simple continuum description of solvation using emerging data on the dielectric response of ionic liquids. A preliminary report of some of these results has already appeared.[45]

The remainder of this work is organized as follows. After describing the experimental methods in section 2, the results

Special Issue: B: Paul F. Barbara Memorial Issue

Received: June 3, 2012
Revised: August 5, 2012

dx.doi.org/10.1021/jp305430a | J. Phys. Chem. B XXXX, XXX, XXX−XXX

Table 1. Ionic Liquids Studied[a]

ID	IL	CAS RN	chemical name	source	OD
21	$[Im_{21}][DCA]$	370865-89-7	1-ethyl-3-methylimidazolium dicyanamide	Iolitec (>98%)	0.48*
22	$[Im_{21}][BF_4]$	143314-16-3	1-ethyl-3-methylimidazolium tetrafluoroborate	Iolitec (>98%)	0.22
24	$[Im_{21}][TfO]$	145022-44-2	1-ethyl-3-methylimidazolium triflate	Merck/EMD Chemicals	0.13
I2	$[Im_{21}][Tf_2N]$	174899-82-2	1-ethyl-3-methylimidazolium bis(trifluoromethylsulfonyl)imide	Iolitec (99%)	0.06
41	$[Im_{41}][DCA]$	448245-52-1	1-butyl-3-methylimidazolium dicyanamide	Richard Buchner[91]	0.07
42	$[Im_{41}][BF_4]$	174501-65-6	1-butyl-3-methylimidazolium tetrafluoroborate	Iolitec (99%)	0.03
43	$[Im_{41}][PF_6]$	174501-64-5	1-butyl-3-methylimidazolium hexafluorophosphate	Iolitec (99%)	0.11
44	$[Im_{41}][TfO]$	174899-66-2	1-butyl-3-methylimidazolium trifluoromethanesulfonate	Iolitec (99%)	0.35*
I4	$[Im_{41}][Tf_2N]$	174899-83-3	1-butyl-3-methylimidazolium bis(trifluoromethylsulfonyl)imide	Kanto Chemical	0.02
46	$[Im_{41}][FAP]$	917762-91-5	1-butyl-3-methylimidazolium tris(pentafluoroethyl) trifluorophosphate	Merck/EMD Chemicals	0.41*
I6	$[Im_{61}][Tf_2N]$	382150-50-7	1-hexyl-3-methylimidazolium bis(triflluoromethylsulfonyl)imide	Iolitec (99%)	0.38*
I8	$[Im_{81}][Tf_2N]$	178631-04-4	1-methyl-3-octylimidazolium bis(triflluoromethylsulfonyl)imide	Iolitec (99%)	0.30*
I0	$[Im_{10,1}][Tf_2N]$	433337-23-6	1-decyl-3-methylimidazolium bis(trifluoromethylsulfonyl)imide	Iolitec (>98%)	0.11*
P3	$[Pr_{31}][Tf_2N]$	223437-05-6	1-methyl-1-propyl pyrrolidinium bis(trifluoromethanesulfonyl)imide	Gary Baker[92,93]	0.03
P4	$[Pr_{41}][Tf_2N]$	223437-11-4	1-butyl-1-methylpyrrolidinium bis(trifluoromethanesulfonyl)imide	Gary Baker[92,93]	0.01
P5	$[Pr_{51}][Tf_2N]$	380497-17-6	1-methyl-1-pentyl pyrrolidinium bis(trifluoromethanesulfonyl)imide	Gary Baker[92,93]	0.05
P6	$[Pr_{61}][Tf_2N]$	380497-19-8	1-hexyl-1-methylpyrrolidinium bis(trifluoromethanesulfonyl)imide	Gary Baker[92,93]	0.01
P8	$[Pr_{81}][Tf_2N]$	927021-43-0	1-methyl-1-octyl pyrrolidinium bis(trifluoromethanesulfonyl)imide	Gary Baker[92,93]	0.04
P0	$[Pr_{10,1}][Tf_2N]$	1003581-49-4	1-decyl-1-methylpyrrolidinium bis(trifluoromethanesulfonyl)imide	Gary Baker[92,93]	0.01
M1	$[N_{2000}][NO_3]$	22113-86-6	ethylammonium nitrate	this work[94] and Iolitec	0.17
M2	$[S_{222}][Tf_2N]$	321746-49-0	triethylsulfonium bis(trifluoromethylsulfonyl)imide	Iolitec (99%)	0.01

[a]ID is a code used in figures and IL the abbreviation used to designate ionic liquids throughout the paper. CAS RN is the Chemical Abstracts registry number. OD is the optical density of the neat IL at 400 nm in a 1 cm path used as an indication of the optical purity of the IL. Asterisks here denote that TCSPC experiments were run in a front-face geometry with a 1 mm path length cell.

are discussed in four parts. Section 3A involves the energetics of solvation. New measurements made here, combined with the compilation made previously,[22] provide a survey of the free energies and reorganization energies of C153 in some 35 different ionic liquids. Consistent with prior work,[22] we find these energetic quantities to be best correlated to the mean ion separation (or ion concentration). Section 3B discusses the spectral or solvation response functions observed. We find the response to be bimodal and well represented by a subpicosecond Gaussian component plus a broadly distributed component having the form of a stretched exponential function. As previously noted, the parameters describing these two components are found to be respectively related to inertial ion characteristics[40,42] and hydrodynamic[19,22,24,42,43] properties of the liquids. In section 3C we compare the present results with the few prior measurements of the complete solvation response of C153 and other probes. Finally, in section 3D we compare the observed solvation response to what is predicted based on a simple dielectric continuum theory. We find that, whereas the predicted and observed response functions are qualitatively similar, the model systematically overestimates the speed of the solvation by a factor of at least 2−4.

2. EXPERIMENTAL METHODS

Coumarin 153 (laser grade) was obtained from Lambda Physik and Exciton and used as received. The 21 ionic liquids surveyed in this work and their origins are listed in Table 1. The majority of these liquids were the highest purity commercially available. Several liquids were synthesized by Gary Baker, Richard Buchner, or by us, and in these cases references to the synthetic procedures are provided in the table. Apart from drying, the liquids were used as received except for $[Im_{41}][BF_4]$ and $[Im_{41}][PF_6]$ which were treated with activated carbon to remove colored impurities. The liquids were all dried in vacuum to water levels of less than 100 ppm by weight prior to use.

Samples for steady-state and time-correlated single photon counting (TCSPC) measurements were prepared in vials and then transferred to either 1 cm or 1 mm sealed quartz cuvettes. Flowing solutions were used for fluorescence upconversion (FLUPS) measurements. The latter solutions were protected from water in a Perspex box flushed with argon and pumped through a thin optical cell which could also be oscillated perpendicular to the beam direction. (See Figure S1 in the Supporting Information.) With this arrangement, samples typically maintained water levels of <200 ppm over the course of an experiment (approximately 5 h). However, in the cases of $[Im_{21}][BF_4]$ and $[Im_{41}][DCA]$, final water contents were near 1000 ppm. In these liquids 1000 ppm corresponds to about one water molecule per 100 ion pairs. We do not anticipate that water even at this level will significantly alter the results reported here. This assertion is supported by experiments in $[Im_{21}][BF_4]$. For this ionic liquid we made seven different runs having varying water contents between 650 and 5000 ppm (0.5−4 mol %) but observed no systematic differences as a function of water content. FLUPS and absorption measurements were carried out at room temperature (20.5 ± 0.5) °C. Steady-state fluorescence and TCSPC measurements were performed in temperature controlled cells at 20.5 ± 0.1 °C.

Steady-state and ps/ns time-resolved fluorescence measurements were performed in the same manner detailed in ref 22. The only difference was that when significant impurity fluorescence was present (denoted with asterisks in the OD column of Table 1) 1 mm cuvettes were used and emission collected in a front-face geometry. In these cases, C153 concentrations providing ODs of near 1 were used in order to minimize the effect of impurity fluorescence. Otherwise ODs of 0.1−0.2 for a 1 cm path length were employed. Excitation at 400 nm for TCSPC measurements was supplied by the doubled output of a cavity-dumped Ti:sapphire laser which delivers ~150 fs pulses at a repetition rate of 5.4 MHz. Emission was

dx.doi.org/10.1021/jp305430a | J. Phys. Chem. B XXXX, XXX, XXX−XXX

Table 2. Summary of Peak Frequencies and Energies[a]

no.	IL	$\nu_{abs}/10^3$ cm^{-1}	$\nu_{em}/10^3$ cm^{-1}	$\nu(0)/10^3$ cm^{-1}	$\nu(\infty)/10^3$ cm^{-1}	$-\Delta_{sol}G$ /kJ mol^{-1}	λ_{sol} /kJ mol^{-1}
21	$[Im_{21}][DCA]$	23.27	18.29	20.37	18.29	47.2 ± 1.1	12.7 ± 0.9
22	$[Im_{21}][BF_4]$	23.64	18.24	20.68	18.25	45.2 ± 1.4	14.9 ± 1.2
24	$[Im_{21}][TfO]$	23.53	18.39	20.59	18.38	45.4 ± 1.1	13.8 ± 0.9
I2	$[Im_{21}][Tf_2N]$	23.59	18.57	20.65	18.57	43.7 ± 1.1	12.8 ± 0.9
41	$[Im_{41}][DCA]$	23.28	18.40	20.48	18.41	46.3 ± 1.4	12.7 ± 1.2
42	$[Im_{41}][BF_4]$	23.44	18.44	20.63	18.41	45.7 ± 1.0	14.2 ± 0.8
43	$[Im_{41}][PF_6]$	23.48	18.59	20.66	18.49	45.2 ± 0.9	13.0 ± 0.7
44	$[Im_{41}][TfO]$	23.51	18.52	20.58	18.49	44.7 ± 1.1	12.9 ± 0.9
I4	$[Im_{41}][Tf_2N]$	23.51	18.65	20.68	18.62	43.7 ± 0.8	11.7 ± 0.6
46	$[Im_{41}][FAP]$	23.56	18.85	20.62	18.80	43.5 ± 1.1	12.1 ± 0.9
I6	$[Im_{61}][Tf_2N]$	23.55	18.79	20.59	18.74	43.0 ± 1.1	11.5 ± 0.9
I8	$[Im_{81}][Tf_2N]$	23.57	18.92	20.61	18.82	42.2 ± 1.1	11.0 ± 0.9
I0	$[Im_{10,1}][Tf_2N]$	23.62	19.04	20.64	18.86	41.5 ± 1.1	10.8 ± 0.9
P3	$[Pr_{31}][Tf_2N]$	23.70	18.70	20.84	18.67	42.7 ± 0.8	13.2 ± 0.6
P4	$[Pr_{41}][Tf_2N]$	23.66	18.78	20.82	18.74	41.9 ± 1.0	11.9 ± 0.8
P5	$[Pr_{51}][Tf_2N]$	23.64	18.89	20.70	18.81	41.9 ± 1.1	11.7 ± 0.9
P6	$[Pr_{61}][Tf_2N]$	23.58	18.90	20.71	18.81	42.8 ± 0.8	11.4 ± 0.6
P8	$[Pr_{81}][Tf_2N]$	23.59	19.05	20.71	18.92	41.5 ± 1.1	11.0 ± 0.9
P0	$[Pr_{10,1}][Tf_2N]$	23.63	19.22	20.73	19.02	40.7 ± 0.8	10.8 ± 0.6
M1	$[N_{2000}][NO_3]$	22.98	18.24	20.44	18.25	49.3 ± 2.2	13.0 ± 1.8
M2	$[S_{222}][Tf_2N]$	23.63	18.63	20.68	18.61	43.1 ± 1.1	12.7 ± 0.9

[a] ν_{abs}, ν_{em}, $\nu(0)$, and $\nu(\infty)$ denote the peak frequencies of the absorption, steady-state emission, "time-zero" emission, and the extrapolated value of the time-dependent emission spectrum, respectively. $\Delta_{sol}G$ and λ_{sol} are calculated from such frequencies using eqs 1 and 2 and a 2:1 weighted average of peak and first moment frequencies.

collected though an ISA H10 monochromator with a bandpass of 8 nm and over a time window of 20 ns. The overall response time of the TCSPC instrument was 25−30 ps (fwhm), as measured using a scattering solution. Emission decays were recorded at more than 20 wavelengths spanning the emission spectrum and these decays independently fit to a multiexponential form using an iterative reconvolution algorithm in order to partially remove the effects of instrumental broadening. Reconstucted time-resolved spectra were obtained from these fitted decays according to the methods described in ref 46.

Femtosecond time-resolved emission measurements were made with a home-built broadband fluorescence upconversion spectrograph[47,48] which supplies emission spectra over the range 425−750 nm. The experiment is based on a Ti:sapphire laser (Femtolasers sPro) which provides 30 fs, 500 μJ pulses at 800 nm and a 500 Hz repetition rate. The output of this laser system is split into two beams with intensities in a ratio of 6:1. Pulses of 430 μJ energy drive an optical parametric amplifier (TOPAS, Light Conversion) which delivers 60 μJ, 1340 nm pulses in horizontal polarization used for optical gating. For optical pumping, the rest of the fundamental light is frequency doubled to 400 nm pulses whose polarization is set parallel to the gate with a half wave plate. After passing a triple mirror on a variable delay stage, attenuated pump pulses (~1 μJ) are focused by a thin lens onto the sample cell to a spot diameter of about 0.1 mm. To obtain a good optical image with the subsequent collection optics, the sample cell is made with two 0.2 mm thickness windows, which are typically spaced 0.2−0.3 mm apart. Sample ODs near 1.5 at 400 nm were used. Fluorescence was refocused by an off-axis Schwarzchild objective and collected by a concave mirror onto a KDP crystal for upconversion. The procedures used for spectral correction and evaluation are described in detail in ref 48. The temporal response of the FLUPS experiment is given by the fwhm ≈ 80 fs of the Gaussian fits of the time trace of pump scatter from pure methanol.

In experiments with the ionic liquid ethylammonium nitrate a photoinduced reaction, which produced a red-brown solid, was observed in the FLUPS, but not in the TCSPC experiments. NMR measurements indicated the presence of two unidentified reaction products. To avoid this reaction, we found it necessary to use a single-pass flow system in which the C153 + ionic liquid was discarded after passing once through the sample cell rather than recirculating it in the manner used for all of the remaining FLUPS experiments.

3. RESULTS AND DISCUSSION

A. Solvation Energies. Before examining solvation dynamics, we consider the energetics of the $S_0 \leftrightarrow S_1$ transition of C153 in different ionic liquids. The solvent contributions to the free energy difference $\Delta_{solv}G$ and the reorganization energy λ_{solv} associated with the $S_0 \leftrightarrow S_1$ transition of C153 can be calculated from

$$\Delta_{sol}G = \frac{1}{2}h[\nu_{abs} + \nu(\infty)] - \Delta G_0 \quad (1)$$

$$\lambda_{sol} = \frac{1}{2}h[\nu(0) - \nu(\infty)] \quad (2)$$

In these equations ν_{abs}, $\nu(0)$, and $\nu(\infty)$ represent some measure of the frequency of the absorption, "time-zero" emission, and fully equilibrated emission, respectively, and ΔG_0 is the estimated gas-phase energy difference, 296 kJ/mol.[22] Peak frequencies used to calculate these quantities are summarized in Table 2. The time-zero frequency $\nu(0)$ is an approximation for the hypothetical vibrationally equilibrated emission spectrum that would be observed before any solvent relaxation. It is determined using steady-state spectra of C153 in the nonpolar reference solvent 2-methylbutane, as described

dx.doi.org/10.1021/jp305430a | J. Phys. Chem. B XXXX, XXX, XXX−XXX

in ref 49. The equilibrated emission frequency $\nu(\infty)$ is determined by extrapolating time-resolved TCSPC data using a stretched exponential fit (see below). As can be seen from the data in Table 2, this frequency is in all cases within 200 cm^{-1} to the red of the steady-state emission frequency ν_{em}. Values of $\Delta_{solv}G$ and λ_{solv} in Table 2 were derived by combining data from peak and first moment frequencies.

Figure 1 shows these energies plotted versus the inverse of the mean ion separation $d = (V_m/N_A)^{1/3}$ where V_m is the molar volume and N_A Avogadro's number. This figure expands the data set of ionic liquids used to make a similar comparison in a prior study.[22] As used previously, $1/d$ is a coarse measure of the strength of electrostatic interactions in a given liquid, based on the idea that the lattice energy of a neat ionic liquid should scale with d^{-1} and that solvation energies should be inversely related to an effective cavity size comprising both solute and solvent contributions. As illustrated in Figure 1, variations in both $\Delta_{solv}G$ and λ_{solv} with ionic liquid appear to be reasonably correlated to the inverse of this mean ion separation. Also shown in the bottom panel of Figure 1 (dashed curve) is the solute size dependence recently derived from simulations of spherical ionic and dipolar solutes in a model ionic liquid.[32] The empirical relationship found in those simulation and shown here is $\lambda_{solv} \cong A/(0.4R_u + 0.2R_v)^3$ where R_u is the solute radius (3.9 Å using van der Waals increments[50]) and $R_v \cong d/2$ is a mean ion radius.[51] This simulated dependence appears to reproduce the observed data slightly better than a simple d^{-1} dependence.

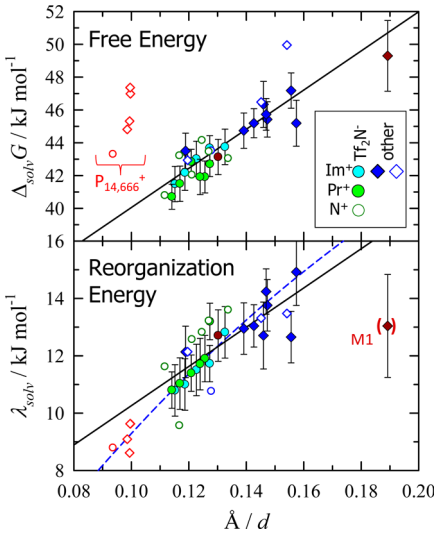

Figure 1. Solvation contributions to the free energy change and reorganization energy associated with the $S_0 \leftrightarrow S_1$ transition of C153 versus the inverse of the mean ion separation, $1/d$. Filled symbols correspond to the data in Table 2 whereas open symbols are data on additional ionic liquids reported in ref 22. Blue and cyan points are data in imidazolium ionic liquids (Im^+), light green are pyrrolidinium (Pr^+), and dark green ammonium ionic liquids (N^+). Red points denote ionic liquids containing the trihexyltetredecylphosphonium cation, and circles denote bis(trifluoromethanesulfonyl)imide ionic liquids. Lines are fits to all data excluding the phosphonium liquids: $\Delta_{solv}G = 28.1 - 101/d$ ($N = 30$, $R = 0.89$) and $\lambda_{solv} = 3.4 - 59/d$ ($N = 29$, $R = 0.77$). The dashed line in the bottom panel shows the size-dependence found in MD simulations (see text).

We note that there are several outliers in Figure 1. The reorganization energy of ethylammonium nitrate ("M1"), which is comprised of the smallest ions studied here, is much smaller than expected based on these trends. It is also an outlier in terms of dynamical properties discussed in the next section. We do not understand the reason for these deviations, but as already noted, photochemical degradation occurred in this, the only protic ionic liquid studied. Also, as noted in previous work,[22] values of $\Delta_{solv}G$ in ionic liquids based on the highly alkylated phosphonium cation tetradecyltrihexylphoshonium ($P_{14,666}^+$) do not follow the same correlation established by the remaining ionic liquids. A much larger change in solvation energy (and slower solvation[22]) is observed, which we conjecture reflects a change of environment between S_0 and S_1 made possible by the extensive domain structure of these phosphonium ionic liquids.[52,53]

We note that $\Delta_{solv}G$ should be sensitive to solvent electronic polarizability as well as to the "nuclear polarizability" represented by d^{-1}. We therefore also explored correlations of $\Delta_{solv}G$ (and for completeness λ_{solv}) incorporating the solvent refractive index. However, the refractive indices of the liquids studied span a small range (1.43 ± 0.03), and no improvement in the correlations was found. The same can be said of the relative permittivities, ε_r. Except for ethylammonium nitrate (ε_r = 28.3 ± 0.5[54]), the relative permittivities available for 15 of the 21 liquids listed in Table 2 all fall in a range characteristic of moderately polar conventional solvents $\varepsilon_r = 16 \pm 2$.[54]

B. Spectral/Solvation Response Functions. Figure 2 shows representative time-resolved emission spectra of C153 in $[Pr_{51}][Tf_2N]$. In the top panel are broad-band spectra recorded with the FLUPS technique and in the middle panel spectra reconstructed from TCSPC decays (points). Both types of data were fit with log-normal line shape functions (smooth curves in both panels) in order to parametrize the time evolution of the spectra.[46] The bottom panel of Figure 2 shows the level of agreement typically observed between spectra obtained with

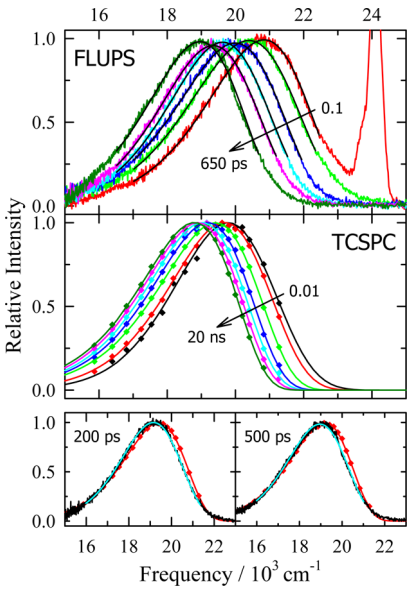

Figure 2. Time-resolved emission spectra of C153 in $[Pr_{51}][Tf_2N]$. The top panel show FLUPS data and the middle panel spectra reconstructed from TCSPC decays. The spike near 24 000 cm^{-1} is due to residual scattering of the gate pulse. The smooth curves in both panels are fits of the data to log-normal functions. The bottom panels compare the TCSPC (red) and FLUPS (black with cyan fit) spectra at two times.

dx.doi.org/10.1021/jp305430a | J. Phys. Chem. B XXXX, XXX, XXX–XXX

FLUPS and TCSPC over the time range where both spectra are expected to be reliable. Figure 3 displays the behavior of two

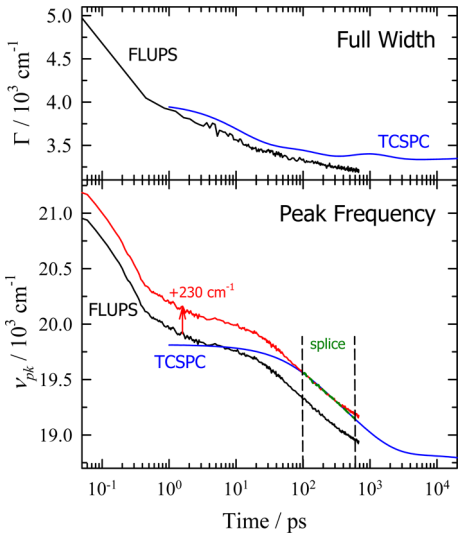

Figure 3. Time evolution of the spectral width (fwhm; $\Gamma(t)$) and peak frequency $\nu_{pk}(t)$ obtained from log-normal fits of the FLUPS and TCSPC spectra in Figure 2, illustrating how a combined data set is obtained. (See text.)

log-normal parameters derived from the spectra in Figure 2, the width $\Gamma(t)$ (fwhm) and the peak frequency $\nu_{pk}(t)$. As illustrated in the top panel of Figure 3, we typically observe a substantial (~1000 cm^{-1}) decrease in the width of the spectrum at times less than 100 ps. Recent work in conventional solvents demonstrates that this width change is due primarily to vibrational cooling when significant excess energy is used for excitation (~3000 cm^{-1} here).[55] As has been done in past work, we will ignore this effect and focus on the evolution of the peak frequency $\nu_{pk}(t)$ to monitor the solvation response. Specifically, we extract the spectral response function

$$S_\nu(t) = \frac{\nu_{pk}(t) - \nu_{pk}(\infty)}{\nu_{pk}(0) - \nu_{pk}(\infty)} \quad (3)$$

and equate it to the solvation response, the normalized function describing relaxation of the solute−solvent interaction energy difference. The solvation response functions obtained in this manner are contaminated to some degree by the vibrational effect, but we anticipate that the distortions so produced will not be greater than other sources of uncertainty in the data.

As shown in the bottom panel of Figure 3, the peak frequencies measured in the FLUPS and TCSPC experiments are not in perfect agreement. In the case illustrated here, there is a 230 cm^{-1} mismatch between the two frequencies over the time range 100−600 ps, where we expect both methods to be reliable. These data are representative of most of the data collected here in that the average absolute discrepancy is 270 cm^{-1} for the 21 data sets reported. The sign of the deviation is random (the signed average is 30 cm^{-1}), and we attribute it to the variability in the spectrum of the gating light used in the FLUPS experiments. Because the TCSPC data are referenced to calibrated steady-state spectra, we take the TCSPC frequencies as being correct and shift the FLUPS spectra to best match over the 100−600 ps range. To smoothly splice together the two sets of data, a weighted average of the shifted FLUPS and TCSPC frequencies is used. The weighting assigns the FLUPS data 100% weight at 100 ps and the TCSPC data 100% weight at 600 ps with a linear interpolation between these limits.

Composite $\nu_{pk}(t)$ data generated in this fashion are shown in Figure 4 for the two homologous series of ionic liquids

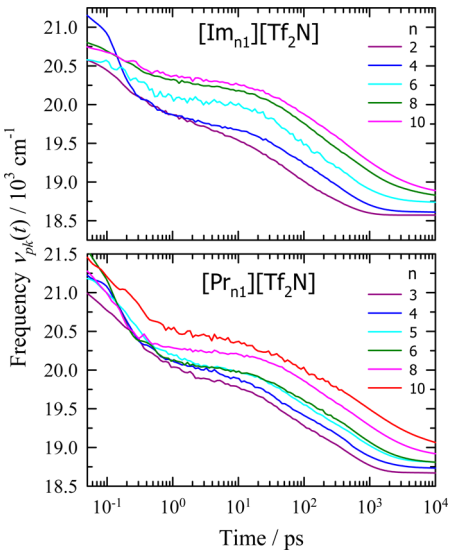

Figure 4. Time evolution of the peak frequencies $\nu_{pk}(t)$ of C153 in the imidazolium $[Im_{n1}][Tf_2N]$ and pyrrolidinium $[Pr_{n1}][Tf_2N]$ series of ionic liquids.

$[Im_{n1}][Tf_2N]$ and $[Pr_{n1}][Tf_2N]$. Given that one expects systematic behavior as a function of alkyl chain length n in such series, these data provide some indication of the uncertainties present in the $\nu_{pk}(t)$ data. At times greater than 10 ps, systematic behavior is observed in both series. Between 100 ps and 1 ns the $\nu_{pk}(t)$ data parallel one another to better than 100 cm^{-1} and there is an orderly progression of the limiting frequencies $\nu_{pk}(\infty)$. At times below 1 ps the data are not as orderly, and below 300 fs the various curves cross in unexpected ways. In the case of the $[Im_{n1}][Tf_2N]$ series it is only the n = 4 data that appear to misbehave, whereas in the $[Pr_{n1}][Tf_2N]$ series the data are randomly ordered at 100 fs. We interpret these observations to indicate that uncertainties in the $\nu_{pk}(t)$ data are roughly ±100 cm^{-1} at times greater than 1 ps and as large as ±400 cm^{-1} at 100 fs. With Stokes shift magnitudes of ~2000 cm^{-1} these uncertainties translate into uncertainties in $S_\nu(t)$ of ±5% at most times and up to ±20% at subpicosecond times. Due to the large uncertainty in some early time data, in order to convert $\nu_p(t)$ data to spectral response functions, we used the values of $\nu_{pk}(0)$ obtained from steady-state estimates as described in the previous section. In the majority of the data sets (16/21 cases) the mean absolute deviation of ν_{pk} at 50 fs from the estimated $\nu_{pk}(0)$ is 170 cm^{-1} (8% of the predicted Stokes shift). In most of these cases the observed frequency was slightly less than that predicted, as would be expected based on the finite time resolution of the experiment. However, in the $[Pr_{n1}][Tf_2N]$ series for n > 3 (5 data sets) the observed frequencies at early time exceeded the time-zero estimates by an average of nearly 600 cm^{-1} (29%). The reason for the large discrepancies in these particular solvents is not known.

Representative spectral/solvation response functions $S_\nu(t)$ are provided in Figure 5. As is clear from this figure and from the previous $\nu_{pk}(t)$ plots, the solvation response is strongly

dx.doi.org/10.1021/jp305430a | J. Phys. Chem. B XXXX, XXX, XXX−XXX

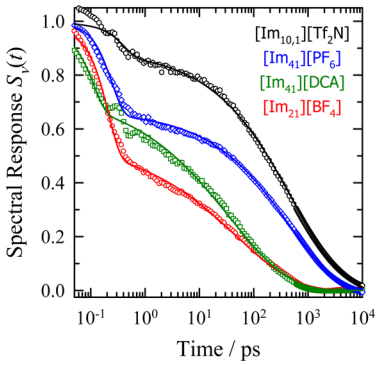

Figure 5. Representative spectral response functions (points) and fits to eq 4 (solid curves).

biphasic, consisting of a subpicosecond component followed by another component that extends from a few picoseconds out to nanosecond times. A convenient way of characterizing this biphasic response is through fits of the $S_\nu(t)$ data to a Gaussian + stretched exponential form

$$S_\nu(t) = f_G \exp\left\{-\frac{1}{2}\omega_G{}^2 t^2\right\} + (1 - f_G)\exp\{-(t/\tau)^\beta\} \quad (4)$$

Example fits are shown as the smooth curves in Figure 5. In all cases, this simple functional form suffices to represent the observed data to within anticipated uncertainties.[56] Table 3 summarizes the fit parameters for all of the ionic liquids studied here. Also listed in Table 3 under the heading "Q" is a rough assessment of the relative quality of the data sets based on a number of indicators: the frequency shift required to match the FLUPS and TCSPC data, the similarity of the data in the splicing region, and the level of agreement between observed and predicted time-zero frequencies. $Q = 1$ represents the most reliable data.

Before discussing the fit parameters, some comment is necessary concerning the values of ω_G obtained here. We have not attempted to deconvolute the FLUPS data in order to remove the effects of the 80 fs (fwhm) instrumental response function (IRF). This IRF width corresponds to a Gaussian frequency of $\omega_{IRF} = 8.7$ ps^{-1} and one might anticipate that observed values of ω_G near to ω_{IRF} would be significantly reduced from their true values by instrumental broadening. Assuming both the fast response and the IRF to be Gaussian functions of time, one would expect $\omega_{obs}{}^{-2} = \omega_{true}{}^{-2} + \omega_{IRF}{}^{-2}$, and thus values of $\omega_G > \omega_{IRF}$ would not be observed. But, as seen from Table 3, we do find $\omega_G > \omega_{IRF}$ in a number of cases. The reason is that we use an independent means of establishing $\nu_{pk}(0)$, which forces the fit of $S_\nu(t)$ to account in an approximate way for the shortfalls in $\nu_{pk}(t \rightarrow 0)$ caused by instrumental broadening. This approach appears to provide the best means of extracting short-time information from the current data and we believe that the fitted values of ω_G reported in Table 3 should provide reasonable estimates even for $\omega_G > \omega_{IRF}$. In support of this claim we note that the values determined here are consistent with simulation estimates[29,30,32,57] as well as with experimental data collected with much higher time resolution[40] discussed in the following section.

We now consider the extent to which the parameters f_G, ω_G, $\langle\tau\rangle_G$, β, and $\langle\tau\rangle_{str}$ correlate with various properties of the ions comprising the ionic liquids or with bulk liquid properties. The times $\langle\tau\rangle_G$ and $\langle\tau\rangle_{str}$ are integral times associated with the Gaussian and stretched exponential components ($\langle\tau\rangle_G = (\pi/2)^{1/2}\omega_G^{-1}$ and $\langle\tau\rangle_{str} = \tau\Gamma(\beta^{-1})/\beta$). The ion properties examined include the cation (C) an anion (A) masses and van der Waals radii, R_C and R_A, the reduced mass of a C+A pair, μ, and the

Table 3. Parameters Characterizing the $S_\nu(t)$ Response[a]

no.	IL	Q	f_G	ω_G/ps^{-1}	$\langle\tau\rangle_G$/ps	τ/ns	β	$\langle\tau\rangle_{str}$/ns
21	$[Im_{21}][DCA]$	1	0.18 ± 0.08	14 ± 3.0	0.09	0.009	0.34	0.051 ± 0.010
22	$[Im_{21}][BF_4]$	1	0.45 ± 0.08	6.7 ± 1.3	0.19	0.05	0.40	0.16 ± 0.03
24	$[Im_{21}][TfO]$	1	0.39 ± 0.08	7.8 ± 1.6	0.16	0.20	0.41	0.61 ± 0.12
I2	$[Im_{21}][Tf_2N]$	2	0.25 ± 0.08	6.2 ± 1.2	0.20	0.06	0.44	0.15 ± 0.04
41	$[Im_{41}][DCA]$	1	0.27 ± 0.08	12 ± 2.5	0.10	0.04	0.40	0.12 ± 0.02
42	$[Im_{41}][BF_4]$	2	0.34 ± 0.08	7.0 ± 1.4	0.18	0.17	0.48	0.37 ± 0.11
43	$[Im_{41}][PF_6]$	1	0.33 ± 0.08	5.8 ± 1.2	0.22	0.45	0.50	0.90 ± 0.18
44	$[Im_{41}][TfO]$	2	0.37 ± 0.08	6.7 ± 1.3	0.19	0.24	0.50	0.48 ± 0.14
I4	$[Im_{41}][Tf_2N]$	3	0.39 ± 0.15	4.1 ± 1.6	0.31	0.19	0.60	0.29 ± 0.12
46	$[Im_{41}][FAP]$	1	0.21 ± 0.08	2.8 ± 0.6	0.44	0.23	0.51	0.44 ± 0.09
I6	$[Im_{61}][Tf_2N]$	3	0.22 ± 0.08	4.7 ± 0.9	0.27	0.25	0.55	0.41 ± 0.17
I8	$[Im_{81}][Tf_2N]$	2	0.13 ± 0.11	3.1 ± 0.9	0.41	0.40	0.52	0.76 ± 0.23
I0	$[Im_{10,1}][Tf_2N]$	1	0.11 ± 0.08	3.4 ± 0.7	0.37	0.55	0.49	1.13 ± 0.23
P3	$[Pr_{31}][Tf_2N]$	1	0.32 ± 0.08	3.9 ± 0.8	0.32	0.14	0.49	0.29 ± 0.06
P4	$[Pr_{41}][Tf_2N]$	2	0.33 ± 0.11	3.3 ± 1.0	0.38	0.21	0.54	0.37 ± 0.11
P5	$[Pr_{51}][Tf_2N]$	2	0.29 ± 0.15	2.3 ± 0.9	0.55	0.31	0.56	0.51 ± 0.15
P6	$[Pr_{61}][Tf_2N]$	2	0.32 ± 0.15	2.8 ± 1.1	0.45	0.42	0.58	0.66 ± 0.20
P8	$[Pr_{81}][Tf_2N]$	3	0.22 ± 0.15	3.4 ± 1.4	0.37	0.59	0.56	0.98 ± 0.39
P0	$[Pr_{10,1}][Tf_2N]$	3	0.16 ± 0.15	1.1 ± 0.4	1.16	0.82	0.53	1.49 ± 0.60
M1	$[N_{2000}][NO_3]$	3	0.39 ± 0.08	8.1 ± 1.6	0.16	0.03	0.45	0.062 ± 0.012
M2	$[S_{222}][Tf_2N]$	2	0.28 ± 0.11	3.0 ± 0.9	0.42	0.07	0.54	0.13 ± 0.04

[a] "Q" represents the quality of the experimental data with 1 being the best (see text). f_G, ω_G, β, and τ are the fit parameters of eq 4 used to describe $S_\nu(t)$ data. $\langle\tau\rangle_G$ and $\langle\tau\rangle_{str}$, the integral times of the Gaussian and stretched exponential components, serve to characterize the time scales of the two components of the response.

dx.doi.org/10.1021/jp305430a | J. Phys. Chem. B XXXX, XXX, XXX−XXX

"inertial factor" $(R_C + R_A)^{3/2}\mu^{1/2}$ introduced in ref 42. Bulk liquid properties tested were the molar volume and viscosity.[58] (Table S1 of the Supporting Information lists many of these properties.) Only weak correlations were found between f_G and any of the quantities examined. Given the fact that estimated uncertainties in f_G ($\pm 0.1 - 0.15$) are a large proportion of its range, this result is not surprising. Nevertheless it is clear from Table 3 that f_G decreases with increasing alkyl chain length n in the two series $[Im_{n1}][Tf_2N]$ and $[Pr_{n1}][Tf_2N]$. The time scale of the subpicosecond component of the response, characterized by ω_G or $t_G^{(1/e)}$, is most strongly correlated to the C+A reduced mass, anion mass, and the inertia factor. As noted in previous work,[40,42] without pointing to any particular solvation mechanism, such correlations confirm the inertial character of this ultrafast component, as predicted by numerous simulation studies.[27,29,30,32,59] Figure 6 illustrates the best of these

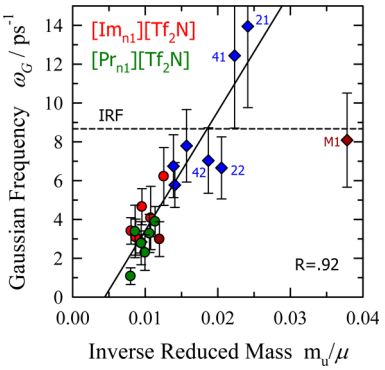

Figure 6. Correlation of the Gaussian frequency ω_G with the inverse of the cation+anion reduced mass. Circles indicate ionic liquids with the Tf_2N^- anion, diamonds are other anions. Red and green symbols denote the $[Im_{n1}][Tf_2N]$ and $[Pr_{n1}][Tf_2N]$ series, respectively, blue symbols are liquids with Im_{n1}^+ cations and dark red symbols M1 and M2. Numbers indicate ionic liquids as listed in Table 1. The line is a fit to all of the data except M2, 20 points correlation coefficient = 0.92.

correlations, that between ω_G and μ^{-1}. The dashed line labeled "IRF" in this figure is a reminder of the 80 fs instrumental response time of the FLUPS experiment. With the exception of the data in ethylammonium nitrate (M1) which is excluded from the fit, the correlation is quite good. This correlation would predict a much higher Gaussian frequency for ethylammonium nitrate than is observed. As already discussed, the predicted magnitude of the Stokes shift (or reorganization energy, Figure 1) in this solvent is also much smaller than expected relative to other solvents. These two deviations are likely to be related and warrant further study.

The slow component of the solvation response, measured by $\langle\tau\rangle_{str}$, is most strongly correlated to the solvent viscosity η. Figure 7 displays this correlation, which can be represented by a power law, $\langle\tau\rangle_{str} \propto \eta^p$ with $p = 1.2 \pm 0.2$. This type of near proportionality of the integral solvation time to viscosity in a single ionic liquid versus temperature[21,24,60,61] and within collections of ionic liquids[19,22,42,24,43,61,62] has been reported numerous times previously. In the present case it appears to hold to within uncertainties for the two homologous series $[Im_{n1}][Tf_2N]$ and $[Pr_{n1}][Tf_2N]$, but when all liquids are considered one sees a number of outliers, most notably $[Im_{21}][TfO]$ ("24") and ethylammonium nitrate ("M1"). This correlation between the time of the slow solvation component and viscosity presumably reflects the fact that solvation is

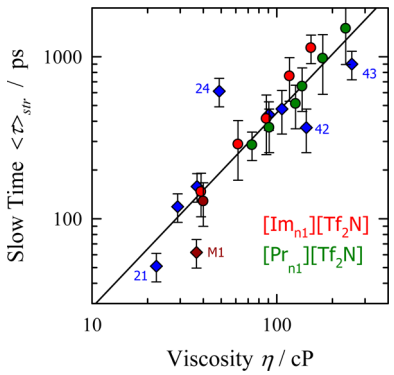

Figure 7. Dependence of the integral time associated with the stretched exponential component upon solvent viscosity. Circles indicate ionic liquids with the Tf_2N^- anion, and other symbols are other anions. Red and green symbols denote data from the $[Im_{n1}][Tf_2N]$ and $[Pr_{n1}][Tf_2N]$ series, respectively, blue symbols are liquids with Im_{n1}^+ cations, and dark red symbols are M1 and M2. The line shows the correlation $\langle\tau\rangle_{str}/ps = 1.8(\eta/cP)^{1.2}$.

associated with structural relaxation of the solvent as found in computer simulations.[32] One additional relationship, not previously noted, can be found in the data in Table 3. There is a fairly good correlation ($R = -0.84$) between the dispersity of the slow solvation component, represented by the stretching exponent β, and the Gaussian frequency ω_G (Figure S2). The interpretation of this observation is unclear.

C. Comparison to Prior Determinations of $S_\nu(t)$. Of the many studies using time resolution insufficient to observe the shorter components of $S_\nu(t)$, we consider only the previous survey of C153 solvation from one of our laboratories.[22] Eight of the ionic liquids measured here were also examined in that previous work. The samples and, in many cases, their sources differed in the two studies, moreover the temperature used previously was 25 °C rather than the 20.5 °C used here. Nevertheless, when the TCSPC data from the two studies are fit to stretched exponential functions and the fit parameters compared, good agreement is generally found. For example, the integral solvation times $\langle\tau\rangle_{str}$ (200−1800 ps) in the two studies are linearly correlated, with a correlation coefficient of 0.991 and standard error of 80 ps for values ranging between 200 and 1800 ps. The stretching exponents determined in the two studies β show a mean absolute deviation of 0.08. These comparisons provide additional measures of the reproducibility of the long-time portions of the response.

There are five prior studies reporting observation of the complete solvation response[37,38,42−44,63] to which we can compare with the present $S_\nu(t)$ data. A tabulation of some features of these studies (Table S2) and graphical comparisons with the present $S_\nu(t)$ data (Figure S3) are provided in the Supporting Information. We find that agreement with most prior results is reasonably good, once differences in time resolution are accounted for. Three groups previously used C153 as a solute. Hander et al.[37] measured the Stokes shift dynamics of C153 in ethylammonium nitrate ($[N_{2000}][NO_3]$) with 300 fs time resolution. Their results for this particular liquid agree with the present results to within estimated uncertainties. Lang et al.[38] measured C153 in two ionic liquids not studied here. Their results are unusual in that they report Stokes shifts of only ~500 cm^{-1} in marked disagreement with the present data[63] and that of other workers.[44,62,64,65] Lastly, Kimura et al. recently reported Stokes shift dynamics of C153

dx.doi.org/10.1021/jp305430a | J. Phys. Chem. B XXXX, XXX, XXX−XXX

Table 4. Sources of Dielectric and Other Data Used for $S_\nu(t)$ Prediction[a]

no.	S	IL	frequency range	ε_0	ε_∞	n_D	$\varepsilon_\infty - n_D^2$	σ_0/S m^{-1}	label	$\varepsilon(\nu)$ source	n_D source	σ_0 source
21	S	$[Im_{21}][DCA]$	100 MHz to 10 THz	11.0	2.5	1.510	0.2	2.20	B	71	95	96
22	S	$[Im_{21}][BF_4]$	100 MHz to 10 THz	15.9	1.94	1.411	−0.1	1.55	B	71	97	98
			10 MHz to 20 GHz	13.6	6.7	1.411	4.7	1.52	N	79	79	79
24	S	$[Im_{21}][TfO]$	500 MHz to 10 THz	17.7	2.12	1.432	0.1	0.98	B	73	97	96
I2		$[Im_{21}][Tf_2N]$	100 MHz to 90 GHz	12.9	3.18	1.423	1.2	0.90	B	74	99	100
			10 MHz to 20 GHz	12.3	4.7	1.421	2.7	0.95	N	79	79	79
			200 MHz to 20 GHz	12.3	3.23	1.423	1.2	0.83	W	75	99	75
41	S	$[Im_{41}][DCA]$	100 MHz to 3 THz	11.3	2.13	1.509	−0.1	1.052	B1	69	101	98
			100 MHz to 10 THz	12.3	2.36	1.509	0.1	1.052	B2	71	101	98
42	S	$[Im_{41}][BF_4]$	100 MHz to 3 THz	12.2	2.15	1.422	0.1	0.35	B	74	102	98
			10 MHz to 20 GHz	14.1	5.45	1.421	3.4	0.44	N	79	79	79
			200 MHz to 20 GHz	11.0	4.08	1.422	2.1	0.30	W	76	102	76
43	S	$[Im_{41}][PF_6]$	100 MHz to 3 THz	11.8	2.1	1.410	0.1	0.15	B	69	102	98
			10 MHz to 20 GHz	14.1	4.8	1.407	2.8	0.165	N	79	79	79
			40 MHz to 40 GHz	12.4	3.26	1.410	1.3	0.16	Y	80	102	80
44	S	$[Im_{41}][TfO]$	100 MHz to 90 GHz	15.6	1.82	1.438	−0.2	0.29	B	74	103	98
I4	S	$[Im_{41}][Tf_2N]$	100 MHz to 90 GHz	12.9	2.23	1.427	0.2	0.39	B	74	99	100
			10 MHz to 20 GHz	13.7	4.25	1.426	2.2	0.42	N	79	79	79
			200 MHz to 20 GHz	11.5	3.03	1.427	1.0	0.37	W	75	99	75
			40 MHz to 40 GHz	12.7	2.7	1.427	0.7	0.37	Y	80	99	75
I6		$[Im_{61}][Tf_2N]$	200 MHz to 89 GHz	12.7	2.58	1.430	0.5	0.22	B	70	99	100
			10 MHz to 20 GHz	14.1	4.8	1.430	2.8	0.226	N	79	79	79
I8		$[Im_{81}][Tf_2N]$	10 MHz to 20 GHz	16.8	3.72	1.432	1.7	0.14	N	79	79	79
P4	S	$[Pr_{41}][Tf_2N]$	200 MHz to 10 THz	12.1	2.33	1.423	0.3	0.26	B	74	93	77
			200 MHz to 20 GHz	11.7	2.42	1.423	0.4	0.26	W	77	93	77
M1	S	$[N_{2000}][NO_3]$	500 MHz to 12 THz	28.5	2.52	1.452	0.4	2.50	B	72	104	78
			10 MHz to 1 THz	26.4	3.2	1.452	1.1	2.50	K	78	104	78
M2	S	$[S_{222}][Tf_2N]$	100 MHz to 3 THz	14.7	2.2	1.426	0.2	0.512	B	74	this work	77
			200 MHz to 20 GHz	13.2	1.83	1.426	−0.2	0.711	W	77	this work	77

[a]The column labeled S indicates select dielectric data sets for which essentially the complete dielectric response is observed. ε_0 and ε_∞ are the limiting values of ε' derived from the fitted $\varepsilon(\nu)$ data, n_D is the refractive index, and σ_0 is the static conductivity. "Label" indicates the labels used in the figures.

in $[Im_{41}][PF_6]$ and $[Im_{41}][Tf_2N]$ at 40 °C with 800 fs time resolution.[44] Their response functions closely parallel ours over the range 10 ps to 10 ns but differ at shorter times in a manner expected given the differences in temperature and time resolution.

Measurements using two other solvatochromic probes have also been reported. Arzhantsev et al. measured the Stokes shift dynamics of 4-dimethylamino-4′-cyanostilbene (DCS) in four common ionic liquids with 450 fs time resolution.[42] Previous comparisons between C153 and DCS suggested that at least the long-time components of the solvation response are nearly the same. (See Figure 1 of ref 42.) The present comparisons show that the $S_\nu(t)$ response functions of C153 and DCS are very similar at times longer than ∼10 ps, except in the case of $[Im_{41}][PF_6]$. We note that in the DCS study $[Im_{41}][PF_6]$ stood out among the 6 ionic liquids studied as being more distributed in time (Figure 5, $\beta = 0.31$) which is not the case here. Kimura measured the solvation dynamics of 4′-*N*,*N*-diethylamino-3-methoxyflavone (DEAMF) in three of the liquids examined here with 650 fs time resolution.[43] If one assumes that some of the spectral shift was missed in these experiments and renormalizes the data to agree at 10 ps, in $[Im_{21}][Tf_2N]$ and $[Im_{41}][Tf_2N]$ there is remarkably good agreement with the present results for $t > 10$ ps whereas in $[Im_{41}][PF_6]$ the long-time agreement is poor. These comparisons between the C153 and two other solutes suggest that the diffusive solvation component is relatively insensitive to solute in the case of these large fluorophores. Previous studies with picosecond time resolution[19,66] also provided some evidence for this invariance, but additional experiments are needed to confirm this suggestion.

In addition to dynamic Stokes shift measurements, Muramatsu et al. recently reported 3-pulse photon echo peak shift (3PEPS) experiments on the chromophore oxazine 4.[40] The 3PEPS technique[67,68] is well suited to measuring the linear response equivalent of the spectral response function on much shorter time scales (>50 fs) than can be reliably measured using fluorescence methods. After filtering out the oscillatory contributions of intramolecular dynamics, Muramatsu et al. extracted the fastest components (to 100 ps) of the spectral response functions of six imidazolium (and one phosphonium) ionic liquids. As found here,[42] they found that the fastest time constants were related to inertial characteristics of the anions or ion-pairs of the liquids. Four of the liquids in the present work can be directly compared with results of this 3PEPS study: $[Im_{21}][Tf_2N]$, $[Im_{41}][BF_4]$, $[Im_{41}][PF_6]$, and $[Im_{41}][Tf_2N]$. The shortest times observed in the two experiments ($\langle\tau\rangle_G$ in this work and τ_1 in 3PEPS) for these liquids are respectively (0.20 ± 0.05 and 0.22 ± 0.02), (0.18 ± 0.04 and 0.11 ± 0.01), (0.22 ± 0.04 and 0.15 ± 0.01), and (0.31 ± 0.12 and 0.21 ± 0.01). Although the present times average ∼35% longer than the 3PEPS times, differences are close to the combined uncertainties in all cases. This comparison provides some confidence that we are indeed extracting meaningful values of

dx.doi.org/10.1021/jp305430a | J. Phys. Chem. B XXXX, XXX, XXX−XXX

ω_G and also that the 3PEPS measurements are observing the equivalent of the solvation response.

D. Comparisons to Dielectric Continuum Predictions. We now examine to what extent one can use the dielectric dispersion data recently collected on neat ionic liquids[69−80] to predict the solvation response measured here with C153. We adopt the simplest dielectric continuum model for this comparison. The solute is treated as a point dipole centered in a spherical cavity of dielectric constant $\varepsilon_u = 2$, which represents its polarizability. The solvent is treated as a continuum fluid having a generalized dielectric response function $\hat{\eta}(\nu)$. This model and the calculations involved are essentially the same as those described in ref 42 and previous work.[36] Normalized response functions are determined using the expressions[45]

$$S_{dc}(t) = \frac{L_p^{-1}\{[\hat{\chi}(p) - \hat{\chi}(0)]/p\}}{\hat{\chi}(\infty) - \hat{\chi}(0)} \quad (5)$$

$$\hat{\chi}(p) = \frac{\hat{\eta}(p) - 1}{\hat{\eta}(p) + \frac{1}{2}\varepsilon_u} \quad (6)$$

where L_p^{-1} denotes an inverse Laplace transform with respect to the variable $p = 2\pi i\nu$. In contrast to ref 42, where the contribution of conductivity was erroneously neglected, the dielectric function used here is the generalized function

$$\hat{\eta}(\nu) = \hat{\varepsilon}(\nu) + \frac{2i\sigma_0}{\nu} \quad (7)$$

This function describes what is actually measured in experiments, whereas $\hat{\varepsilon}(\nu)$, the remainder after the diverging conductivity contribution is removed, is what is typically reported.[81,69]

Dielectric relaxation data are currently available for 14 of the 21 ionic liquids studied here. The data are primarily from the groups of Buchner[69−74] and Weingärtner,[75−78] as summarized in Table 4. Listed in this table are frequency ranges over which data were collected. The upper limit of this range has a significant impact on the quality of the solvation predictions possible. To capture the majority of the intermolecular dynamics of relevance to solvation, $\hat{\varepsilon}(\nu)$ must extend to terahertz frequencies. For only 9 of the solvents are such extended frequency data available. As shown by the column labeled $\Delta\varepsilon = \varepsilon_\infty - n_D^2$ in Table 4, in the remaining cases, some portion of the dielectric spectrum is missed. Although the fraction missed, $(\varepsilon_\infty - n_D^2)/(\varepsilon_0 - n_D^2)$, is typically <25%, its absence hampers prediction of the short-time response. Moreover, neglect of this component can also significantly alter the long time behavior of the predicted response.

Figure 8 illustrates the effect that missing high-frequency components of $\hat{\varepsilon}(\nu)$ have on the calculated solvation response as well as our method of accounting for this effect. Figure 8a shows the dielectric response of $[Im_{41}][Tf_2N]$ as parametrized by four groups.[74,75,79,80] Over the frequency range 200 MHz ≥ ν ≥20 GHz where all data sets overlap there is reasonable agreement among three of the four sets of results. The data of Mizoshiri et al.[80] ("Y") deviate significantly from that of the other workers, and the same is true of their data in the other three ionic liquids in Table 4. We therefore do not include these data in the comparisons to follow. Although none of the dielectric data on $[Im_{41}][Tf_2N]$ extend to the THz frequencies, the data of Buchner and co-workers,[74] recorded to 90 GHz, detects the presence of a resonance component in $\hat{\varepsilon}(\nu)$ which

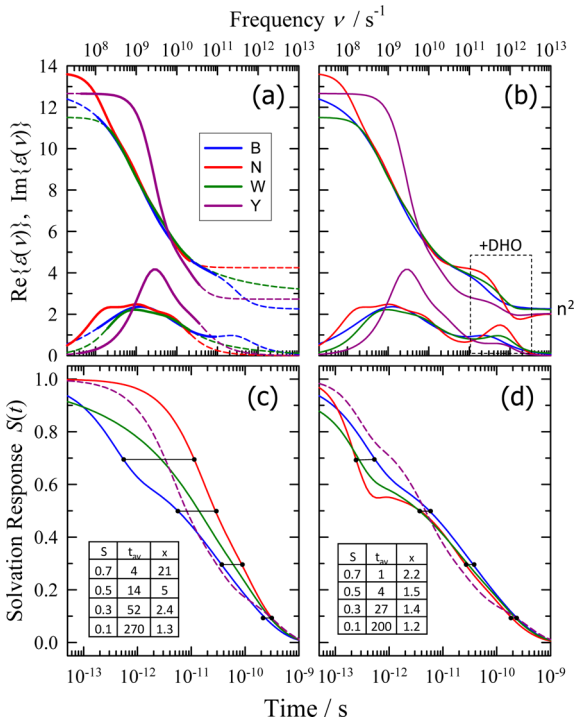

Figure 8. Solvation response functions derived from various parametrizations of dielectric dispersion data $\varepsilon(\nu)$ for $[Im_{41}][Tf_2N]$. The sources (labeled B, N, W, and Y) are listed in Table 4. Panel a shows the $\varepsilon(\nu)$ data as reported, with thick curves indicating the range over which data were collected and the dashed curves the parametrized fits to the data. Panel b shows these same data after inclusion of an additional resonance term (eq 8). Panel c shows solvation response functions $S(t)$ calculated using the dielectric data in panel a and eqs 5−7, whereas panel d shows the corresponding functions based on the "corrected" dielectric data in panel b. The tie lines in panels c and d show the spread of times required for $S(t)$ to decrease to values of 0.7, 0.5, 0.3, and 0.1. The inset tables show the average time t_{av} (ps) and the ratio of longest to shortest times x to reach these values of S (excluding the dashed curves Y).

gives rise to a peak near 250 GHz in $Im\{\hat{\varepsilon}(\nu)\}$. This additional term, absent in the other parametrizations, is responsible for the close approach of $\hat{\varepsilon}(\nu)$ to n_D^2 at high frequencies, i.e. for the small value $\Delta\varepsilon = 0.2$ for the "B" data set listed Table 4. In the remaining cases, where the fraction of the dielectric response missed is larger, we introduce an ad hoc correction term in the form of a damped harmonic oscillator

$$\Delta\hat{\varepsilon}(p) = (\varepsilon_\infty - n_D^2)\frac{\nu_0^2}{\nu_0^2 + p(p+\gamma)} \quad (8)$$

to account for the missing response. Based on surveying the available high-frequency dielectric data we adopt the somewhat arbitrary values $\nu_0 = 1$ THz and $\gamma = 2$ THz to use in applying this correction to all ionic liquids in which $\Delta\varepsilon/n_D^2 > 10\%$. Dielectric functions corrected in this manner are shown in Figure 8b.

Solvation response functions computed from these dielectric data are shown in the bottom panels of Figure 8. In Figure 8c are plotted functions calculated using the dielectric parametrizations directly as reported whereas Figure 8d shows the results obtained after adding the correction term. If one uses the dielectric data without accounting for missing components of $\hat{\varepsilon}(\nu)$, the predicted $S(t)$ functions that differ considerably,

dx.doi.org/10.1021/jp305430a | J. Phys. Chem. B XXXX, XXX, XXX−XXX

not only at short times, but even out to times of hundreds of picoseconds. Inclusion of the correction term described by eq 8 brings the predictions into much closer agreement. At times greater than ~1 ps the correction essentially collapses the predictions using the dielectric data of refs 79 (red) and 75 (green) onto the prediction made using the uncorrected data of Buchner and co-workers[74] (blue). (Use of the Mizoshiri data[80] (dashed curve) provides a corrected $S(t)$ curve that is also not far from the other predictions, but its long-time behavior differs from that of the other three.) Given the fact that the parameters used in eq 8 are only generic values one would not expect the correction to be quantitative. Nevertheless, the three solid curves in panel d agree to within a factor of 2 even at subpicosecond times. Overall the comparison in Figure 8d (and similar comparisons for other ionic liquids[45]) suggests that reliable predictions of $S(t)$ can be made even in the absence of complete frequency coverage of the dielectric response.

Comparisons of dielectric continuum predictions to observed solvation response functions are provided for eight ionic liquids in Figure 9. (Figure S3 shows comparable plots for the

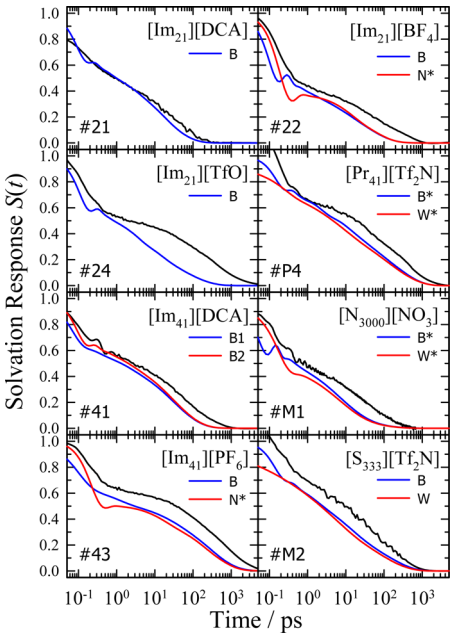

Figure 9. Comparison of observed spectral/solvation response functions (black curves) with predictions of the dielectric continuum model embodied in eqs 5−8. Labels B, N, and W indicate the sources of dielectric data according to Table 4. Asterisks indicate cases where an additional resonance term (eq 8) was added.

remaining six liquids.) In most cases the shapes of the observed and calculated response functions are similar when plotted in this semilogarithmic format. The relative amplitudes of the fast and slow components are comparable, and after ~1 ps the observed and calculated curves closely parallel one another, except in the case of $[Im_{21}][TfO]$ (see below). The only qualitative difference is that weak, subpicosecond oscillations are predicted in some cases, for example in $[Im_{21}]$ [DCA], $[BF_4]$, and [TfO]. Such oscillations are not present in the observed response functions. (Note that when a resonance component is added to the dielectric data as indicated by asterisks in Figure 9, oscillations may be produced in $S_\nu(t)$ but this aspect of the predictions is not trustworthy.) As in the case of simulated data,[32] despite the oscillations in some of the predicted $S(t)$ functions, a Gaussian + stretched exponential fit (eq 4) usually captures the main features of the predicted functions. We first use the parameters derived from fits to eq 4 to provide a more quantitative comparison between the predicted and observed dynamics.

Figure 10 shows the results of such a comparison using the 11 selected dielectric data sets indicated by an "S" in column 2

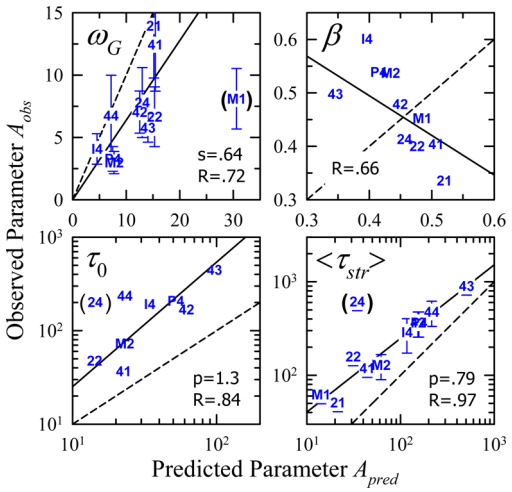

Figure 10. Comparison of parameters obtained by fitting predicted and observed $S(t)$ data to eq 4. The parameters plotted are ω_G/ps^{-1}, β, τ/ps, $\langle\tau_{str}\rangle$/ps. Symbols indicate particular ionic liquids as defined in Table 1. Solid lines are regressions to either $A_{obs} = sA_{pred}$ (ω_G) or $\ln(A_{obs}) = a + p\ln(A_{pred})$ (times). Values of s, p, and the correlation coefficient R are indicated. (Values of a are 0.16 and 1.88 for τ and $\langle\tau_{str}\rangle$, respectively.) Dashed lines indicate $A_{obs} = A_{pred}$. Points shown in parentheses were not included in the regressions.

of Table 4. These data are selected based on the fact that the frequency coverage is sufficient that either no correction or a minimal correction ($[Pr_{41}][Tf_2N]$ and $[N_{2000}][NO_3]$) for missing components is required. The Gaussian fractions f_G (not shown) derived from fitting mostly range between 0.2 and 0.4. Although the predicted and observed values of f_G are poorly correlated, they fall within experimental uncertainties of one another in 9 of 11 cases. Figure 10 shows that predicted values of ω_G are close to observed values in all cases except ethylammonium nitrate (M1). In ethylammonium nitrate the dielectric continuum predictions as well as the correlations in Figures 1 and 6 suggest that the present experiments are missing a substantial part of what is expected to be a very fast ($\omega_G \approx 30$ ps^{-1}) inertial component. For the 10 remaining solvents the observed values of ω_G are approximately 2/3 of those predicted by the dielectric continuum treatment. The observed and predicted parameters of the stretched exponential term in eq 4, representing the slow component of the observed dynamics, are similar. The values of the stretching exponent β are mostly predicted to fall in the range 0.3−0.5, whereas most observed values are slightly higher, between 0.4 and 0.6. As shown in Figure 10, there is a curious anticorrelation between β_{obs} and β_{pred} whose meaning is unclear. Perhaps the best overall measure of the slow component of solvation is the integral time of the stretched exponential term, $\langle\tau_{str}\rangle$. With the exception of #24 = $[Im_{21}][TfO]$ there is an excellent correlation between the observed and predicted times, but the predicted times are an average of 2.8 times faster than those observed. We note that the deviation shown here is not as large

dx.doi.org/10.1021/jp305430a | J. Phys. Chem. B XXXX, XXX, XXX−XXX

as reported in a previous comparison[42] where the effect of conductivity was erroneously neglected in the dielectric calculations.

An alternative way of examining the relationship between the predicted and observed response functions is to compare the times required for $S(t)$ to reach particular levels. Figure 11

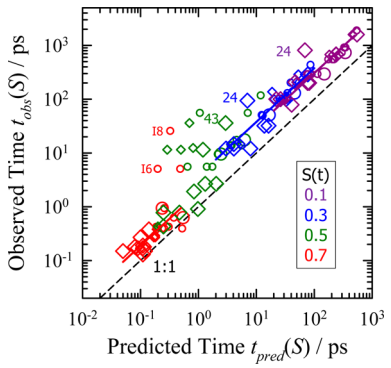

Figure 11. Comparison of observed $S(t)$ times versus times predicted using the dielectric continuum model. Different colors indicate the times required for $S(t)$ to reach the levels indicated. Large symbols indicate comparisons made with "select" dielectric data. The dashed line labeled 1:1 indicates equality of times and the solid lines average ratios of times (see text).

shows a comparison including all 14 solvents listed in Table 4 (27 data sets).[48] Plotted here are times at the $S(t)$ levels 0.1, 0.3, 0.5, and 0.7. (See Figure 8.) These various $S(t)$ levels approximately report on dynamics taking place in different time regimes. $S = 0.7$ reports primarily on subpicosecond dynamics, $S = 0.5$ and 0.3 on intermediate times of 1−100 ps, and $S = 0.1$ on the slowest (>100 ps) dynamics present. What is suggested by the plots in Figure 9 is confirmed in Figure 11. With almost no exceptions, the response functions predicted by the dielectric continuum model decay faster than the observed functions. For the $S = 0.1$, 0.3, and 0.7 levels the correlation between $t_{pred}(S)$ and $t_{obs}(S)$ is generally good. There is much more scatter in the case of $S = 0.5$ because the changeover from inertial to diffusive dynamics typically occurs when $0.4 \geq S(t) \geq 0.6$ and in this region $S(t)$ is flatter than in most other time regions. Also, as can be seen in Figure 4(d), the addition of a resonance component based on eq 8 can have a large impact on $S(t)$ in this region. In the other three regions, the colored lines indicate average values of the ratio $t_{obs}(S)/t_{pred}(S)$ to be 1.9 ± 0.8 for $S = 0.7$ (omitting #I6 and I8), 3.8 ± 1.2 for $S = 0.3$, and 2.8 ± 0.8 for $S = 0.1$ (omitting #24).

The exceptional cases omitted from this averaging deserve brief comment. The very large departures in the short-time behavior shown by $[Im_{61}][Tf_2N]$ and $[Im_{81}][Tf_2N]$ (#I6 and I8) result from the presence of a pronounced plateau region in the observed response of these systems which is not present to the same extent in the predicted $S(t)$ functions (see Figure S3). In the long-time comparisons ($S = 0.3$ and 0.1), we omit $[Im_{21}][TfO]$ (#24), which deviates significantly from the remaining cases. It was already noted with respect to Figure 7 that the long-time dynamics are much slower than would be predicted based on the viscosity correlation established in other liquids. The correlation times of the select dielectric data exhibit the same behavior as shown in Figure 7 ($\langle\tau_{str}\rangle \propto \eta^{1.2}$) but without $[Im_{21}][TfO]$ deviating from this trend. This difference suggests that something might be wrong with the dynamic Stokes shifts we obtain in $[Im_{21}][TfO]$. We measured virtually the same long-time dynamics with samples of $[Im_{21}][TfO]$ obtained from independent sources, but the results we report for $[Im_{21}][TfO]$ should be considered suspect prior to additional verification.

The above comparisons lead to the following conclusions concerning the applicability of dielectric continuum models for predicting solvation dynamics. The parallelism shown between the observed dynamics and the predictions made with select dielectric data in Figure 9 suggest that the essential solvent motions responsible for solvation are captured in the generalized dielectric spectrum of the neat liquid, $\hat{\eta}(\nu)$. However, both the short-time inertial response and the long-time diffusive dynamics predicted using the simple model described by eqs 5−7 are systematically faster than the observed response, on average by factors of 2−4. Although there are more sophisticated theories of ionic liquid solvation[33−35] which might explain these deviations, we leave it to future work to test their utility. Here we only comment on two approximations made by the simple continuum description that are likely to be inaccurate. The first is the neglect of solute motion. Although solute motion has typically been ignored when considering the dynamics reported by large chromophores like C153 in conventional solvents, simulations[32,45] and molecular theories[83] have shown that solute motion can substantially decrease the time associated with the long solvation component in ionic liquids. (A recent experimental study of several solutes suggested that solute rotation could be significant even in conventional solvents like methanol.[84]) However this effect does not explain the discrepancy between experiment and dielectric continuum predictions. Approximate inclusion of solute motion into the dielectric predictions[85,86] would only make the predictions faster. Simulations suggest[32] that if the solute were actually immobile, as assumed in the above theory, the experimental response would be approximately 2-fold slower, which means that the discrepancy with theory would be significantly worsened.[45]

The second approximation, which does act in the proper direction to explain the discrepancy, is the neglect of the wave-vector (k) dependence of $\hat{\eta}(\nu)$. As discussed in ref 45, the solvation response can be thought of as incorporating charge fluctuations on all length scales, from the large scales ($k = 0$) measured in dielectric experiments to molecular length scales $k \approx \sigma$ where σ is a molecular diameter. What is captured in $\hat{\eta}(\nu) = \hat{\eta}(\nu, k = 0)$, is only the fastest portion of the spectrum of relevant response times[45] present in the full frequency and wave-vector dependent dielectric function $\hat{\eta}(\nu, k)$. It is therefore to be expected that a dielectric continuum model based solely on $\hat{\eta}(\nu, 0)$ would predict solvation dynamics which are too fast, as is observed in this study. We believe this neglect of the wave vector dependence of the dielectric response to be the primary source of the discrepancy between the dielectric predictions and experiment.

4. SUMMARY AND CONCLUSIONS

The combined use of FLUPS and TCSPC techniques has enabled us to capture the complete solvation response of C153 in 21 ionic liquids over the time range 100 fs to 20 ns. The main results and conclusions obtained from this study can be summarized as follows:

1. The additional data on solvation free energies and reorganization energies associated with the $S_0 \leftrightarrow S_1$

dx.doi.org/10.1021/jp305430a | J. Phys. Chem. B XXXX, XXX, XXX−XXX

transition of C153 collected here are consistent with prior work.[22] In a wide variety of ionic liquids, these energies are best correlated to measures of mean ion size or ion concentration,[87] in a manner similar to what is observed in simulation.[32,88] These energies show little connection to the solvent dielectric constant or refractive index.[89]

2. The complete spectral/solvation response functions $S_\nu(t)$ observed here are generally consistent with what has been observed in previous studies employing subpicosecond time resolution.[37,42−44] The response functions are highly bimodal and reasonably described by a rapid Gaussian decay characterized by a frequency ω_G followed by a stretched exponential component typically covering times between 1 ps to and >1 ns. The amplitudes of the subpicosecond component found here, some exceeding 40%, are generally larger than those previously reported,[42−44] likely as a result of the improved time resolution of the present experiments. As in previous studies, we find ω_G or the time scale of the subpicosecond component to be correlated to inertial properties of the solvent ions,[40,42] whereas the integral time of the stretched exponential component is correlated to solvent viscosity.[21,22,24,43,60,61] These connections clearly link the fast component of solvation to some type of inertial dynamics and the slow component to diffusive structural relaxation. Much more detail concerning the molecular mechanisms of solvation are provided by computer simulations. We only mention here that the consensus is that the subpicosecond dynamics involve mostly translational motions of near neighbor ions[27,29,30,32,59] and that the extent of ion motion in the response is remarkably small.[32]
3. In addition to the "ideal" solvation probe C153 only two other solutes[42,43] have been used for complete solvation measurements. Once the effect of time resolution is considered, the direct comparisons between the present C153 data and these other solutes suggests that the solvation response probably does not vary markedly with solute, at least within the type of solute typically used for fluorescence measurements. Nevertheless, the question of solute dependence merits further examination.
4. Comparison of observed $S_\nu(t)$ functions with those predicted based on a simple dielectric continuum model indicates that the molecular dynamics underlying dielectric relaxation and the solvation response are intimately related. However, in contrast to dipolar solvents where the predictions appear to be a good first approximation,[36] in ionic liquids the dielectric predictions are systematically too fast by factors of 2−4. Simulations suggest that the discrepancy would be even larger if it were not for the mitigating effect of solute rotation.[32]

■ ASSOCIATED CONTENT

Supporting Information

Two tables summarizing information about the ionic liquids studied and prior studies of the complete solvation response as well as four figures illustrating details of the flow system used for FLUPS measurements and various comparisons of solvation response functions. This material is available free of charge via the Internet at http://pubs.acs.org.

■ AUTHOR INFORMATION

Corresponding Author

*E-mail: Maroncelli@psu.edu.

Author Contributions

‖These authors contributed equally to this work.

Notes

The authors declare no competing financial interest.

■ ACKNOWLEDGMENTS

The authors would like to thank Gary Baker for preparing the $[Pr_{n1}][Tf_2N]$ ionic liquids, Mohsen Sajadi for critical help performing FLUPS measurements, and Richard Buchner for supplying $[Im_{41}][DCA]$ and for sharing many dielectric results prior to publication. M.L. and M.M. were supported by the Division of Chemical Sciences, Geosciences, and Biosciences, Office of Basic Energy Sciences of the U.S. Department of Energy through Grant DE-FG02-09ER16118. N.P.E. is grateful for support from the Deutsche Forschungsgemeinschaft (priority program "Ionic Liquids"). X-X.Z. thanks the China Scholarship Council for support. M.M. also thanks the Humboldt Foundation for a research fellowship during which this work was initiated.

■ REFERENCES

(1) Stark, A. *Top. Curr. Chem.* **2009**, *290*, 41.
(2) Hallett, J. P.; Welton, T. *Chem. Rev.* **2011**, *111*, 3508.
(3) Sun, P.; Armstrong, D. W. *Anal. Chim. Acta* **2010**, *661*, 1.
(4) Poole, C. F.; Poole, S. K. *J. Sep. Sci.* **2011**, *34*, 888.
(5) Wishart, J. F. *Energy Environ. Sci.* **2009**, *2*, 956.
(6) Tadesse, H.; Luque, R. *Energy Environ. Sci.* **2011**, *4*, 3913.
(7) Armand, M.; Endres, F.; MacFarlane, D. R.; Ohno, H.; Scrosati, B. *Nat. Mater.* **2009**, *8*, 621.
(8) Lin, R.; Taberna, P.-L.; Fantini, S.; Presser, V.; Perez, C. R.; Malbosc, F.; Rupesinghe, N. L.; Teo, K. B. K.; Gogotsi, Y.; Simon, P. *J. Phys. Chem. Lett.* **2011**, *2*, 2396.
(9) Shim, Y.; Jung, Y.; Kim, H. J. *J. Phys. Chem. C* **2011**, *115*, 23574.
(10) Lewandowski, A.; Swiderska-Mocek, A. *J. Power Sources* **2009**, *194*, 601.
(11) Zakeeruddin, S. M.; Graetzel, M. *Adv. Funct. Mater.* **2009**, *19*, 2187.
(12) Kawano, R.; Katakabe, T.; Shimosawa, H.; Nazeeruddin, M. K.; Graetzel, M.; Matsui, H.; Kitamura, T.; Tanabe, N.; Watanabe, M. *Phys. Chem. Chem. Phys.* **2010**, *12*, 1916.
(13) Wishart, J. F.; Castner Edward, W., Jr. *J. Phys. Chem. B* **2007**, *111* (18), 4639.
(14) Wasserscheid, P.; Welton, T., Eds.; *Ionic Liquids in Synthesis*, 2nd ed.; Wiley: New York, 2008.
(15) Endres, F. *Phys. Chem. Chem. Phys.* **2010**, *12*, 1648.
(16) Hynes, J. T. Charge Transfer Reactions and Solvation Dynamics. In *Ultrafast Dynamics of Chemical Systems*; Simon, J. D., Ed.; Kluwer: Dordrecht, The Netherlands, 1994; p 345.
(17) Wishart, J. *J. Phys. Chem. Lett.* **2010**, *1*, 1629.
(18) We provide here only selected reviews or the most recent papers by the various groups active in this field.
(19) Samanta, A. *J. Phys. Chem. B* **2006**, *110*, 13704.
(20) Samanta, A. *J. Phys. Chem. Lett.* **2010**, *1*, 1557.
(21) Ito, N.; Richert, R. *J. Phys. Chem. B* **2007**, *111*, 5016.
(22) Jin, H.; Baker, G. A.; Arzhantsev, S.; Dong, J.; Maroncelli, M. *J. Phys. Chem. B* **2007**, *117*, 7291.
(23) Funston, A. M.; Fadeeva, T. A.; Wishart, J. F.; Castner, E. W. *J. Phys. Chem. B* **2007**, *111*, 4963.
(24) Nagasawa, Y.; Oishi, A.; Itoh, T.; Yasuda, M.; Muramatsu, M.; Ishibashi, Y.; Ito, S.; Miyasaka, H. *J. Phys. Chem. C* **2009**, *113*, 11868.
(25) Carlson, P. J.; Bose, S.; Armstrong, D. W.; Hawkins, T.; Gordon, M. S.; Petrich, J. W. *J. Phys. Chem. B* **2012**, *116*, 503.
(26) Das, S. K.; Sarkar, M. *J. Lumin.* **2012**, *132*, 368.

(27) Shim, Y.; Choi, M. Y.; Kim, H. J. *J. Chem. Phys.* **2005**, *122*, 044511.
(28) Shim, Y.; Kim, H. J. *J. Phys. Chem. B* **2008**, *112*, 11028.
(29) Kobrak, M. N. *J. Chem. Phys.* **2006**, *125*, 64502.
(30) Kobrak, M. N. *J. Chem. Phys.* **2007**, *127*, 184507/1.
(31) Hu, Z.; Margulis, C. J. *J. Phys. Chem. B* **2006**, *110*, 11025.
(32) Roy, D.; Maroncelli, M. *J. Phys. Chem. B* **2012**, *116*, 5951.
(33) Kashyap, H. K.; Biswas, R. *J. Phys. Chem. B* **2008**, *112*, 12431.
(34) Kashyap, H. K.; Biswas, R. *J. Phys. Chem. B* **2010**, *114*, 254.
(35) Song, X. *J. Chem. Phys.* **2009**, *131*, 044503.
(36) Horng, M. L.; Gardecki, J. A.; Papazyan, A.; Maroncelli, M. *J. Phys. Chem.* **1995**, *99*, 17311.
(37) Halder, M.; Headley, L. S.; Mukherjee, P.; Song, X.; Petrich, J. W. *J. Phys. Chem. A* **2006**, *110*, 8623.
(38) Lang, B.; Angulo, G.; Vauthey, E. *J. Phys. Chem. A* **2006**, *110*, 7028.
(39) Oum, K.; Lohse, P. W.; Ehlers, F.; Scholz, M.; Kopczynski, M.; Lenzer, T. *Angew. Chem., Int. Ed.* **2010**, *49*, 2230.
(40) Muramatsu, M.; Nagasawa, Y.; Miyasaka, H. *J. Phys. Chem. A* **2011**, *115*, 3886.
(41) Arzhantsev, S.; Jin, H.; Ito, N.; Maroncelli, M. *Chem. Phys. Lett.* **2006**, *417*, 524.
(42) Arzhantsev, S.; Jin, H.; Baker, G. A.; Maroncelli, M. *J. Phys. Chem. B* **2007**, *111*, 4978.
(43) Kimura, Y.; Fukuda, M.; Suda, K.; Terazima, M. *J. Phys. Chem. B* **2010**, *114*, 11847.
(44) Kimura, Y.; Kobayashi, A.; Demizu, M.; Terazima, M. *Chem. Phys. Lett.* **2011**, *513*, 53.
(45) Maroncelli, M.; Zhang, X.-X.; Liang, M.; Roy, D.; Ernsting, N. P. *Faraday Discuss. Chem. Soc.* **2012**, *154*, 409. Equation 4 in this paper was incorrect. Equation 5 here is the corrected version..
(46) Maroncelli, M.; Fleming, G. R. *J. Chem. Phys.* **1987**, *86*, 6221.
(47) Zhao, L.; Luis Perez Lustres, J.; Farztdinov, V.; Ernsting, N. P. *Phys. Chem. Chem. Phys.* **2005**, *7*, 1716.
(48) Zhang, X.-X.; Wurth, C.; Zhao, L.; Resch-Genger, U.; Ernsting, N. P.; Sajadi, M. *Rev. Sci. Instrum.* **2011**, submitted.
(49) Fee, R. S.; Maroncelli, M. *Chem. Phys.* **1994**, *183*, 235.
(50) Edwards, J. T. *J. Chem. Educ.* **1970**, *47*, 261.
(51) The parameter A is proportional to the square of the dipole moment change $\Delta\mu$ upon excitation. Using a value of $\Delta\mu$ = 7.1 D[90] and the correlation from MD simulations provides $A = 3.0 \times 10^3$ kJ mol^{-1} Å^3. The value of A used to calculate the curve shown in Figure 1 is only 41% of this MD value. Lack of quantitative agreement is not surprising given the fact that C153 is not spherical.
(52) Shimizu, K.; Costa, G. M. F.; Padua, A. A. H.; Rebelo, L. P. N.; Canongia, L. J. N. *J. Mol. Struct.: THEOCHEM* **2010**, *946*, 70.
(53) Kashyap, H. K.; Santos, C. S.; Annapureddy, H. V. R.; Murthy, N. S.; Margulis, C. J.; Castner, E. W., Jr. *Faraday Discuss.* **2012**, *154*, 133.
(54) Huang, M.-M.; Jiang, Y.; Sasisanker, P.; Driver, G. W.; Weingärtner, H. *J. Chem. Eng. Data* **2011**, *56*, 1494.
(55) Sajadi, M.; Ernsting, N. P. 2012, private communication.
(56) Slightly better fits could be achieved using a sum of four exponential functions, but the characteristics of most interest, the amplitudes and integral times associated with the subpicosecond (represented by the Gaussian in eq 4) and the ps-ns (stretched exponential) components were close to those obtained from eq 4. Given the much greater simplicity and interpretability of eq 4, we prefer it for our purposes. We note that this functional form has also recently been shown to provide a convenient means of accurately representing most response functions observed in simulations of model ionic liquids.[32]
(57) Shim, Y.; Kim, H. J. *J. Phys. Chem. B* **2010**, *114*, 10160.
(58) The various ion and liquid properties examined here are not independent and significant correlations are expected among them. One surprise was observation of a strong correlation between the C+A reduced mass and the molar volume of the liquid, R = 0.986 for these 21 assorted ionic liquids.
(59) Shim, Y.; Duan, J.; Choi, M. Y.; Kim, H. J. *J. Chem. Phys.* **2003**, *119*, 6411.
(60) Ingram, J. A.; Moog, R. S.; Ito, N.; Biswas, R.; Maroncelli, M. *J. Phys. Chem. B* **2003**, *107*, 5926.
(61) Arzhantsev, S.; Ito, N.; Heitz, M.; Maroncelli, M. *Chem. Phys. Lett.* **2003**, *381*, 278.
(62) Sanders Headley, L.; Mukherjee, P.; Anderson, J. L.; Ding, R.; Halder, M.; Armstrong, D. W.; Song, X.; Petrich, J. W. *J. Phys. Chem. A* **2006**, *110*, 9549.
(63) Lang et al.[38] measured the Stokes shift of C153 using a combination of 230 fs resolution FLUPS and TCSPC in two ionic liquids. Neither of these liquids were examined here. However, if one compares their reported data on $[Im_{51}][BF_4]$ to the present data on $[Im_{41}][BF_4]$ they appear to be qualitatively quite different. This difference is likely the result of the large difference in the magnitude of the Stokes shift reported in ref 38 (~500 cm^{-1}) and the present work (~2000 cm^{-1}). The origin of this discrepancy remains to be resolved.
(64) Chakrabarty, D.; Hazra, P.; Chakraborty, A.; Seth, D.; Sarkar, N. *Chem. Phys. Lett.* **2003**, *381*, 697.
(65) Mandal, P. K.; Paul, A.; Samanta, A. *Res. Chem. Intermed.* **2005**, *31*, 575.
(66) Ito, N.; Arzhantsev, S.; Maroncelli, M. *Chem. Phys. Lett.* **2004**, *396*, 83.
(67) de Boeij, W. P.; Pshenichnikov, M. S.; Wiersma, D. A. *J. Phys. Chem.* **1996**, *100*, 11806.
(68) Joo, T.; Jia, Y.; Yu, J.-Y.; Lang, M. J.; Fleming, G. R. *J. Chem. Phys.* **1996**, *104*, 6089.
(69) Stoppa, A.; Hunger, J.; Buchner, R.; Hefter, G.; Thoman, A.; Helm, H. *J. Phys. Chem. B* **2008**, *112*, 4854.
(70) Hunger, J.; Stoppa, A.; Schroedle, S.; Hefter, G.; Buchner, R. *ChemPhysChem* **2009**, *10*, 723.
(71) Turton, D. A.; Hunger, J.; Stoppa, A.; Hefter, G.; Thoman, A.; Walther, M.; Buchner, R.; Wynne, K. *J. Am. Chem. Soc.* **2009**, *131*, 11140.
(72) Turton, D. A.; Sonnleitner, T.; Ortner, A.; Walther, M.; Hefter, G.; Seddon, K. R.; Stana, S.; Plechkova, N. V.; Buchner, R.; Wynne, K. *Faraday Discuss.* **2012**, *154*, 145.
(73) Schröder, C.; Sonnleitner, T.; Buchner, R.; Steinhauser, O. *Phys. Chem. Chem. Phys.* **2011**, *13*, 12240.
(74) Buchner, R. 2012, private communication.
(75) Daguenet, C.; Dyson, P. J.; Krossing, I.; Oleinikova, A.; Slattery, J.; Wakai, C.; Weingärtner, H. *J. Phys. Chem. B* **2006**, *110*, 12682.
(76) Schröder, C.; Wakai, C.; Weingärtner, H.; Steinhauser, O. *J. Chem. Phys.* **2007**, *126*, 84511.
(77) Weingartner, H.; Sasisanker, P.; Daguenet, C.; Dyson, P. J.; Krossing, I.; Slattery, J. M.; Schubert, T. *J. Phys. Chem. B* **2007**, *111*, 4775.
(78) Krueger, M.; Bruendermann, E.; Funkner, S.; Weingaertner, H.; Havenith, M. *J. Chem. Phys.* **2010**, *132*, 101101/1.
(79) Nakamura, K.; Shikata, T. *ChemPhysChem* **2010**, *11*, 285.
(80) Mizoshiri, M.; Nagao, T.; Mizoguchi, Y.; Yao, M. *J. Chem. Phys.* **2010**, *132*, 164510/1.
(81) Buchner, R.; Hefter, G. T.; May, P. M. *J. Phys. Chem. A* **1999**, *103*, 1.
(82) The dielectric data of Mizoshiri et al.[80] were excluded from this comparison.
(83) Kashyap, H. K.; Biswas, R. *J. Phys. Chem. B* **2010**, *114*, 16811.
(84) Sajadi, M.; Weinberger, M.; Wagenknecht, H.-A.; Ernsting, N. P. *Phys. Chem. Chem. Phys.* **2011**, *13*, 17768.
(85) Bagchi, B.; Oxtoby, D. W.; Fleming, G. R. *Chem. Phys.* **1984**, *86*, 257.
(86) Kumar, P. V.; Maroncelli, M. *J. Chem. Phys.* **1995**, *103*, 3038.
(87) Kimura, Y.; Hamamoto, T.; Terazima, M. *J. Phys. Chem. A* **2007**, *111*, 7081.
(88) Lynden-Bell, R. M. *J. Chem. Phys.* **2008**, *129*, 204503/1.
(89) Kobrak, M. N.; Li, H. *Phys. Chem. Chem. Phys.* **2010**, *12*, 1922.
(90) Kanya, R.; Ohshima, Y. *Chem. Phys. Lett.* **2003**, *370*, 211.
(91) Fredlake, C. P.; Muldoon, M. J.; Aki, S. N. V. K.; Welton, T.; Brennecke, J. F. *Phys. Chem. Chem. Phys.* **2004**, *6*, 3280.

(92) Baker, S. N.; McCleskey, T. M.; Pandey, S.; Baker, G. A. *Chem. Commun.* **2004**, 940.
(93) Jin, H.; O'Hare, B.; Dong, J.; Arzhantsev, S.; Baker, G. A.; Wishart, J. F.; Benesi, A.; Maroncelli, M. *J. Phys. Chem. B* **2008**, *112*, 81.
(94) Weingaertner, H.; Merkel, T.; Kaeshammer, S.; Schroer, W.; Wiegand, S. *Ber. Bunsen-Ges. Phys. Chem.* **1993**, *97*, 970.
(95) Froeba, A. P.; Kremer, H.; Leipertz, A. *J. Phys. Chem. B* **2008**, *112*, 12420.
(96) Yu, Y.-H.; Soriano, A. N.; Li, M.-H. *J. Chem. Thermodyn.* **2009**, *41*, 103.
(97) Soriano, A. N.; Doma, B. T., Jr.; Li, M.-H. *J. Taiwan Inst. Chem. Eng.* **2010**, *41*, 115.
(98) Zech, O.; Stoppa, A.; Buchner, R.; Kunz, W. *J. Chem. Eng. Data* **2010**, *55*, 1774.
(99) Tariq, M.; Forte, P. A. S.; Gomes, M. F. C.; Lopes, J. N. C.; Rebelo, L. P. N. *J. Chem. Thermodyn.* **2009**, *41*, 790.
(100) Tokuda, H.; Hayamizu, K.; Ishii, K.; Susan, M. A. B. H.; Watanabe, M. *J. Phys. Chem. B* **2005**, *109*, 6103.
(101) Seoane, R. G.; Corderi, S.; Gomez, E.; Calvar, N.; Gonzalez, E. J.; Macedo, E. A.; Dominguez, A. *Ind. Eng. Chem. Res.* **2012**, *51*, 2492.
(102) Soriano, A. N.; Doma, B. T.; Li, M.-H. *J. Chem. Thermodyn.* **2009**, *41*, 301.
(103) Anderson, J. L.; Armstrong, D. W.; Wei, G. T. *Anal. Chem.* **2006**, *78*, 2892.
(104) Greaves, T. L.; Weerawardena, A.; Fong, C.; Krodkiewska, I.; Drummond, C. J. *J. Phys. Chem. B* **2006**, *110*, 22479.